Effects of receptor-mediated endocytosis and tubular protein composition on volume retention in experimental glomerulonephritis

Christian Kastner,[1] Marcus Pohl,[1] Mauricio Sendeski,[2] Gerti Stange,[3] Carsten A. Wagner,[3] Boye Jensen,[4] Andreas Patzak,[2] Sebastian Bachmann,[1] and Franziska Theilig[1]

Institutes of [1]Anatomy and [2]Physiology, Charité-Universitätsmedizin Berlin, Berlin, Germany; [3]Institute of Physiology, University of Zurich, Zurich, Switzerland; and [4]Department of Physiology and Pharmacology, University of Southern Denmark, Odense, Denmark

Kastner C, Pohl M, Sendeski M, Stange G, Wagner CA, Jensen B, Patzak A, Bachmann S, Theilig F. Effects of receptor-mediated endocytosis and tubular protein composition on volume retention in experimental glomerulonephritis. *Am J Physiol Renal Physiol* 296: F902–F911, 2009. First published February 4, 2009; doi:10.1152/ajprenal.90451.2008.—Human glomerulonephritis (GN) is characterized by sustained proteinuria, sodium retention, hypertension, and edema formation. Increasing quantities of filtered protein enter the renal tubule, where they may alter epithelial transport functions. Exaggerated endocytosis and consequent protein overload may affect proximal tubules, but intrinsic malfunction of distal epithelia has also been reported. A straightforward assignment to a particular tubule segment causing salt retention in GN is still controversial. We hypothesized that *1*) trafficking and surface expression of major transporters and channels involved in volume regulation were altered in GN, and *2*) proximal tubular endocytosis may influence locally as well as downstream expressed tubular transporters and channels. Effects of anti-glomerular basement membrane GN were studied in controls and megalin-deficient mice with blunted proximal endocytosis. Mice displayed salt retention and elevated systolic blood pressure when proteinuria had reached 10–15 mg/24 h. Surface expression of proximal Na^+-coupled transporters and water channels was in part [Na^+-P_i cotransporter IIa (NaPi-IIa) and aquaporin-1 (AQP1)] increased by megalin deficiency alone, but unchanged (Na^+/H^+ exchanger 3) or reduced (NaPi-IIa and AQP1) in GN irrespective of the endocytosis defect. In distal epithelia, significant increases in proteolytic cleavage products of α-epithelial Na^+ channel (ENaC) and γ-ENaC were observed, suggesting enhanced tubular sodium reabsorption. The effects of glomerular proteinuria dominated over those of blunted proximal endocytosis in contributing to ENaC cleavage. Our data indicate that ENaC-mediated sodium entry may be the rate-limiting step in proteinuric sodium retention. Enhanced proteolytic cleavage of ENaC points to a novel mechanism of channel activation which may involve the action of filtered plasma proteases.

proximal tubule; collecting duct; megalin; ENaC; NaPi-IIa; AQP1; proteolytic cleavage

PROTEINURIA IS A CLINICAL hallmark of acute and chronic glomerular diseases. Under normal conditions, glomerular perm-selectivity is believed to retain most serum proteins. Only minor quantities especially of albumin are thus passing through the filter to be retrieved by the proximal tubule via receptor-mediator endocytosis (RME), requiring the multiligand receptors megalin and cubilin (15). Proteins are subsequently delivered to the lysosomes, degraded, and finally delivered to the peritubular blood. In nephrotic range proteinuria, substantially more protein is filtered through the damaged glomeruli owing to the general increase in fractional filtration of macromolecules. The resulting high tubular protein concentration leads to saturation of the receptors and exceeds the retrieval and degradation capacity of the proximal tubule, causing cellular protein overload and proteinuria. Interstitial edema, renal salt and water retention, and hypertension occur consequently (17, 35, 42). The potential causes for these disorders have been only partly elucidated to date.

Salt retention in nephrosis has commonly been explained by the hypovolemia concept, implying decreased oncotic pressure following proteinuria, loss of fluid into the interstitium, and subsequent activation of the renin-angiotensin-aldosterone system (RAAS) (18, 32). However, volume disorders in nephrotic patients may also occur without concomitant changes in blood pressure and effects of the RAAS (3, 38). It has therefore been discussed that primary tubular salt retention may per se lead to volume expansion ("circulatory overfilling") (27, 42).

In the search for potential sites of sodium retention along the renal tubule, the proximal tubule has been a focus (1, 4, 24, 34, 51). Protein overload may impair its structure, causing cytoskeletal changes, lipids may become accumulated, and inflammatory factors can be induced. As a result, trafficking of transporters and channels may be impaired (22, 32, 40). Na^+/H^+ exchanger 3 (NHE3)-dependent sodium reabsorption and lysosomal acidification may be affected (7, 32, 34), and coexpressed transport proteins such as aquaporin-1 (AQP1) and the Na^+-P_i cotransporter IIa (NaPi-IIa) may be involved (22).

Distally, regulation of the Na^+-K^+-$2Cl^-$-cotransporter 2 (NKCC2) of thick ascending limbs (TAL) of Henle's loop may be affected as well (32), but the major distal site of retention has formerly been assigned to the collecting ducts (6, 29), and recent work has been concentrated on the activation of the epithelial Na^+ channel (ENaC) in a RAAS-independent way (3, 33, 38). New perspectives have also come from observations that ENaC subunits are cleaved by proteases, which may increase the open probability of the channel (3, 5, 13, 21, 22, 25, 28, 43, 48; for a review, see also Ref. 44).

The aim of this study was to specify possible tubular causes for volume disorders in rapid-progressive, immune-mediated glomerulonephritis (GN) under controlled proteinuria which was clearly below nephrotic range. Changes at the level of the proximal and distal nephron epithelia were analyzed. We

hypothesized that *1*) trafficking and surface expression of the major tubular transport proteins involved in volume regulation were altered in GN, and *2*) proximal tubular RME with respect to its high protein reabsorptive capacity may influence locally as well as downstream expressed tubular transporters and channels. To this end, an established mouse model for anti-glomerular basement membrane (GBM) GN, induced in a kidney-specific, megalin-deficient transgenic strain (36, 51), was used. The partial (50–70%) absence of a functioning, megalin/cubilin-mediated endocytotic apparatus in this strain permits the side-by-side analysis of megalin-deficient and intact proximal tubules for histological analysis and causes low-molecular-weight proteinuria (36). This constellation was used to define the proximal and distal phenotypes of the membrane transporters in GN-grade glomerular proteinuria, with supplementary implications from tubular proteinuria.

METHODS

Animals and treatments. Experiments were performed in female conditional megalin knockout mice (megalin lox/lox; apoE Cre) (51), here termed Cre(+), and in controls (megalin lox/lox), termed Cre(−); body weight 20–30 g, age 12–15 wk. Remnant megalin expression in Cre(+) was verified by sampling of the urinary vitamin D binding protein levels (36). Mice [$n = 25$; 12 Cre(+) mice and 13 Cre(−) mice] were immunologically primed by subcutaneous injection of rabbit IgG in complete Freund's adjuvant. GN was induced 6 days later by the intravenous injection of an anti-mouse GBM serum (47) in six Cre(+) and seven Cre(−) mice, whereas six mice of each strain received an injection of vehicle. The mice were killed when proteinuria had reached 10–15 mg/24 h, and control animals were killed in parallel. Mice were allowed free access to standard chow and tap water. For urine analysis, mice were individually placed in metabolic cages for 24 h before *day 0* and every week starting from *day 12* of the experiment. The experiments were conducted in accordance to the German Law for the protection of animals (Reg G 0178/03).

Blood and urine analyses. Electrolytes in serum and urine were determined by indirect ion-selective electrode measurements (Modular Analytics, Roche Diagnostics, Mannheim, Germany), and urinary osmolality was measured with an osmometer (Gonotec, Berlin, Germany). Blood urea nitrogen (BUN) and creatinine concentrations were quantified enzymatically and by the kinetic Jaffé-method (Modular Analytics, Roche Diagnostics). Creatinine clearance and fractional sodium excretion were calculated using standard equations. Total protein concentration in serum and urine as well as albumin, cholesterol, and triglyceride levels in serum were measured with standardized autoanalyzer methods (Hitachi 747, Hitachi 911, and STA analyzers; Roche Diagnostics).

Hemodynamic measurements. At the end of the experiment, catheters were inserted into the right femoral artery. Blood pressure recordings were performed 24 h after surgery in conscious unrestrained mice. Animals were observed during the recording period, and recording was stopped once an artifact-free recording of at least 5 min was obtained (47).

Fixation and tissue processing for immunohistochemistry. Mice were anesthetized by an injection of pentobarbital sodium (0.06 mg/g body wt ip). Kidneys were then perfused retrogradely through the abdominal aorta using 3% paraformaldehyde (PFA) as described (51) for immunohistochemistry or removed, weighed, and shock-frozen for biochemistry. For cryostat sectioning, tissues were protected from freezing artifacts by subsequent overnight immersion in PBS adjusted to 800 mosmol/kgH$_2$O sucrose, shock-frozen, and stored at −80°C. For the paraffin technique, tissues were postfixed in 3% PFA, dehydrated, and standard paraffin-embedded and stored at −20°C.

Tissue processing for immunoblotting. For isolation of cortical brush border membrane (BBM), the kidney cortex was homogenized in isolation buffer containing 300 mM D-mannitol, 5 mM EGTA, 16 mM HEPES, 10 mM Tris-base, and a protease inhibitor cocktail (Complete, Roche Diagnostics) as described (4). For the isolation of cortical and medullary membrane fractions, tissue was homogenized in sucrose buffer containing 250 mM sucrose, 10 mM triethanolamine, and a protease inhibitor cocktail (Complete) and centrifuged to obtain the plasma membrane fraction. Total protein concentration was measured using the Pierce BCA Protein Assay reagent kit (Pierce, Rockford, IL) and controlled by Coomassie staining.

Gel electrophoresis and SDS-PAGE. After Laemmli's sample buffer was added, the proteins were solubilized at 96°C for 3 min. SDS gel electrophoresis was performed on 8–10% polyacrylamide gels. After electrophoretic transfer of the proteins to nitrocellulose membranes, equity in protein loading and blotting was verified by membrane staining using 0.1% Ponceau red. Membranes were probed overnight at 4°C with primary antibodies and then exposed to horseradish peroxidase-conjugated secondary antibodies (DAKO, Hamburg, Germany). Immunoreactive bands were detected on the basis of chemiluminescence, using an enhanced chemiluminescence kit (Amersham Pharmacia, Freiburg, Germany) before exposure to X-ray films (Hyperfilm, Amersham). For densitometric evaluation of the resulting bands, films were scanned and analyzed using BIO-PROFIL Bio-1D image software (Vilber Lourmat, Marne-La-Vallée, France). All parameters had been normalized to β-actin abundance.

Antibodies. We used previously well-characterized antibodies: rabbit anti-AQP1 (BD Biosciences), monoclonal mouse anti-NHE3 (Chemicon International), rabbit anti-NaPi-IIa, raised against an NH$_2$-terminal peptide sequence; guinea pig anti-megalin (generated against a COOH-terminal peptide), monoclonal mouse anti β-actin (Sigma, Deisenhofen, Germany), rabbit anti-AQP2 (gift from E. Klussmann), monoclonal mouse anti-α$_1$-subunit of Na$^+$-K$^+$-ATPase (α-NKA; Upstate Biotechnology), guinea pig anti-NKCC2 (generated against an NH$_2$-terminal peptide sequence); and α-, β-, and γ-subunits of ENaC (sera produced against NH$_2$-terminal glutathione-*S*-transferase protein of the α-subunit and COOH-terminal glutathione-*S*-transferase proteins of β- and γ-subunits of ENaC), rabbit anti-cyclooxygenase-2 (COX-2; Cayman Chemical), and rabbit anti-renin (gift of A. Kurtz).

Immunohistochemistry. Immunohistochemical staining was performed on cryostat or on paraffin sections. Sections were blocked with 5% skim milk/PBS, incubated with the respective primary antibody (see antibodies listed above), followed by incubation with suitable horseradish peroxidase-coupled secondary antibodies (DAKO) or cy-3-coupled secondary antibodies (Dianova, Hamburg, Germany). In double-labeling techniques, the different primary antibodies were administered consecutively. Specificity of the double-staining procedures was controlled by parallel incubation of consecutive sections, each incubated only with one single probe. Sections were counterstained and analyzed using a Leica DMRB microscope or multilaser confocal scanning microscope (TCS SP-2, Leica Microsystems, Bensheim, Germany).

RNA isolation, reverse transcription, and real-time PCR. Total RNA was extracted from kidney cortices using an RNeasy Mini kit (Qiagen, Hilden, Germany) and treated with DNase I (Invitrogen). Reverse transcription was performed with the Super-Script First-Strand Synthesis System for RT-PCR (Invitrogen). TaqMan Gene Expression Assays were used, and the product IDs for the candidate genes are Mm00431834_m1 (AQP1), Mm01352473_m1 (NHE3), and Mm00441450_m1 (NaPi-IIa). The experiment was performed according to the manual provided by Applied Biosystems (Foster City, CA).

NHE activity measurements. NHE activity was determined in BBM vesicles by the acridine orange technique as described (11). Measurements were performed in a Shimadzu RF-5000 spectrofluometer equipped with a thermostatized cuvette (kept at 25°C). BBM vesicles

were dissolved in a buffer containing 280 mM mannitol, 5 mM Mes, and 2 mM MgCl$_2$ (adjusted to pH 5.5 with N-methyl-D-glucamine). Acridine orange was excited at 493 nm, and emission was monitored at 530 nm. The cuvette was filled with 2 ml of buffer (240 mM mannitol/20 mM HEPES/2 mM MgCl$_2$, adjusted to pH 7.5 with N-methyl-D-glucamine), containing 6 μM acridine orange. The experiment was started by injecting 30 μl of BBM vesicle suspension. After 60 s of equilibration, NHE activity was initiated by injection of 80 μl of 2 M Na gluconate. NHE activity was calculated as the ratio of ΔpH per min over Q, where Q is the initial quenching after injection of BBM vesicles. All experiments were done at least in quadruplicate and repeated four times with BBM vesicles from two animals per experiment. To block specifically NHE3, 100 μM EIPA was used.

Quantification of COX-2 and renin content. Histochemical signals were semiquantitatively evaluated with a ×20 and ×40 objective to establish changes in COX-2 and renin abundance, respectively. The mean number of renin-positive sites or COX-2-positive macula densa cells at the juxtaglomerular apparatus was determined within an area of 100–150 glomeruli on average (49).

Aldosterone assay. Plasma aldosterone was measured with a commercial kit (COAT-A-COUNT, Diagnostic Products). The detection limit was 13.0 pg/ml, and the intra-assay coefficient of variation was <4%.

Presentation of data and statistical analysis. Quantitative data are presented as means ± SE. For statistical comparison, the Mann-Whitney *U*-test was employed. *P* values of <0.05 were considered statistically significant, with (*) demonstrating significance between Cre(−) and Cre(+) and (#) between control and GN mice.

RESULTS

Data. Control mice [Cre(−)] and megalin-deficient mice [Cre(+)] as well as control mice with GN [Cre(−)/GN] and megalin-deficient mice with GN [Cre(+)/GN] were compared. Clinical and renal functional data are presented in Table 1. Control Cre(+) mice had significantly elevated urinary protein

excretion owing to the known low-molecular-weight proteinuria in this strain (36). Application of the nephritogenic antibody to Cre(−) and Cre(+) induced GN with marked proteinuria as established earlier (5). All GN mice had been killed when proteinuria had reached similar levels between strains and tubulointerstitial changes had not yet developed. Baseline blood pressure in Cre(+) was slightly higher than in Cre(−) but did not reach significance (90.2 ± 3.6 vs. 78.2 ± 5.5 mmHg; *P* = 0.10). Induction of GN led to significant blood pressure increases in both strains with a higher tendency maintained in Cre(+)[113.3 ± 6.7 in Cre(−)/GN and 120.3 ± 6.9 in Cre(+)/GN; *P* < 0.05 intrastrain, *P* = 0.12 interstrain] (Fig. 1). Tissue COX-2 and renin immunoreactivity levels, as revealed by juxtaglomerular quantification of histochemical signals, and plasma aldosterone concentrations showed no significant differences between groups (Table 2). The fractional sodium excretion was strongly reduced with GN in both strains (*P* < 0.05). Plasma cholesterol levels were increased in GN. Since Cre(+) had the characteristic mosaic pattern of megalin deficiency (4), the degree of megalin knockout was monitored by Western blotting of BBM, revealing between 50 and 70% megalin deficiency in this strain. Urinary vitamin D binding protein (DBP) excretion was determined to assess the influences of proteinuria and megalin-dependent endocytosis on the tubular handling of this parameter (Fig. 2). As expected, DBP was significantly increased in megalin deficiency [916 ± 99% in Cre(+) vs. 100 ± 32% in Cre(−); *P* < 0.05]. The induction of GN caused a marked increase in DBP excretion in Cre(−)/GN group (782 ± 111%; *P* < 0.05), which was still more pronounced in the Cre(+)/GN (1,371 ± 143%; *P* < 0.05). In sum, RME deficiency alone produced mild proteinuria. The GN groups were characterized by substantial protein-

Table 1. *Clinical parameters*

	Cre(−)	Cre(+)	Cre(−)/GN	Cre(+)/GN
General data				
Body weight, g	21.46±01.34	19.93±1.11	27.40±1.85	28.61±2.00
Kidney weight, g	0.27±0.05	0.29±0.03	0.40±0.04	0.41±0.10
Systolic blood pressure, mmHg	78.20±5.47	90.20±3.55	113.30±3.00†	120.33±6.94†
Water consumption, ml	2.22±0.64	1.54±0.20	1.42±0.18	2.08±0.28
Urinary volume, ml	0.87±0.08	0.67±0.19	1.31±0.23	1.23±0.22
Plasma parameters				
Na$^+$, mmol/l	156.53±01.78	155.95±02.27	153.82±2.05	164.37±6.88
K$^+$, mmol/l	6.86±0.93	5.76±0.53	5.93±0.87	6.69±0.55
Cl$^-$, mmol/l	120.47±2.29	121.32±3.70	117.10±0.83	121.78±2.17
Protein, g/l	43.93±2.72	38.32±6.25	44.34±2.14	32.10±6.90
Albumin, g/l	21.48±1.80	2.74±3.71	21.96±2.07	15.00±2.75
Creatinine, μmol/l	9.40±1.29	9.67±2.60	8.00±2.31	9.13±3.20
Cholesterol, g/l	1.04±0.10	1.04±0.12	1.84±0.10†	1.69±0.21†
Triglyceride, g/l	0.47±0.06	0.43±0.03	0.50±0.03	0.42±0.08
Urea, mmol/l	11.39±3.45	9.15±2.99	10.04±3.21	18.33±3.98
Osmolality, mosmol/kgH$_2$O	337.40±04.36	341.40±7.61	336.60±4.62	357.80±5.30
Renal function				
Creatinine clearance GFR, μl·min^{-1}·g body wt^{-1}	10.87±1.33	11.36±01.92	13.60±1.30	12.60±0.87
Fractional Na$^+$ excretion (FE%)	0.20±0.02	0.31±0.03	0.12±0.01†	0.15±0.01†
Urinary analysis				
Na$^+$, μmol·24 h^{-1}·g body wt^{-1}	3.21±0.48	2.49±0.56	4.49±0.82	4.76±0.68
K$^+$, μmol·24 h^{-1}·g body wt^{-1}	4.22±0.51	3.20±0.59	5.95±0.68	7.46±0.95
Cl$^-$, μmol·24 h^{-1}·g body wt^{-1}	4.67±0.71	2.80±0.75	5.48±1.20	5.11±0.99
Protein, μg·24 h^{-1}·g body wt^{-1}	23.70±3.73	63.75±8.47*	423.59±48.67†	464.97±15.79†
Osmolality, mosmol/kgH$_2$O	1,390±36	1,563±326	1,610±130	1,587±210

Values are means ± SE measured on the last day of the experiment; *n* = 6. Cre(+), conditional megalin knockout mice; Cre(−), controls; GFR, glomerular filtration rate; GN, glomerulonephritis. **P* < 0.05 Cre(−) vs. Cre(+). †*P* < 0.05 control vs. GN.
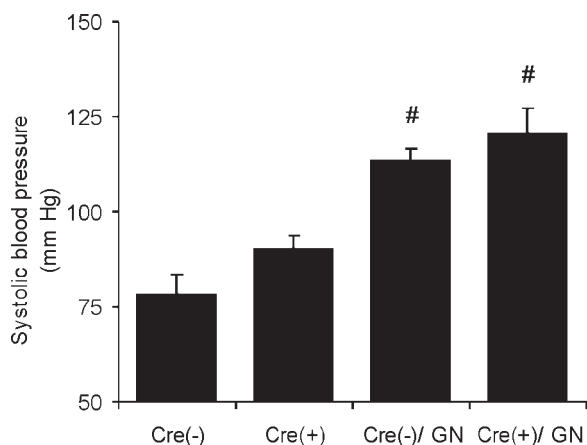
Fig. 1. Systolic blood pressure measurements. Values were significantly increased in control megalin knockout/glomerulonephritis [Cre(−)/GN] and conditional megalin knockout//glomerulonephritis [Cre(+)/GN] mice. The respective numerical values are shown in Table 1. Values are means ± SE, $n = 6$. *$P < 0.05$ for Cre(−) vs. Cre(+). #$P < 0.05$ for control vs. GN.

Fig. 2. Urinary vitamin D binding protein (DBP) excretion. A: Western blot analysis of urinary DBP excretion. Cre(+) show higher levels than Cre(−). Cre(−)/GN and Cre(+)/GN show markedly elevated levels compared with their respective controls. B: densitometric analysis of Western blots. Values are means ± SE, $n = 6$. *$P < 0.05$ Cre(−) vs. Cre(+). #$P < 0.05$ control vs. GN.

uria, elevated blood pressure, proteinuria, and sodium retention; RME deficiency only tangentially but not significantly aggravated these parameters. Juxtaglomerular and RAAS parameters were unchanged.

Abundances of proximal tubular transporters and AQP1. Megalin-positive and megalin-deficient proximal tubule cells were compared side-by-side under control and proteinuric conditions. Figure 3 demonstrates that the absence of megalin and associated changes in cell morphology produced no major changes in NHE3 immunoreactive signals at the base of the BBM, whereas NaPi-IIa and AQP1 signals were increased apically in BBM of Cre(+) compared with Cre(−). NHE3 activity, as measured in BBM vesicles using the acridine orange quenching method, showed no differences between the control groups; using the NHE3-specific inhibitor EIPA (100 μM), total NHE activity was entirely blocked in Cre(−) and Cre(+) alike (Fig. 4). BBM Western blot abundances of NaPi-IIa and AQP1, but not of NHE3 were higher in Cre(+) (Fig. 5A; Table 3), whereas mRNA levels of all three products were unchanged (Table 4).

The induction of GN produced no changes in proximal tubular NHE3 immunoreactive signals irrespective of the presence of megalin (Fig. 3). In contrast, NaPi-IIa and AQP1 signals were markedly decreased in Cre(−)/GN, and in Cre(+)/GN, megalin-positive as well as megalin-negative cells showed reduced signal intensities compared with Cre(+). Total NHE activity in the GN groups was not different from the controls; however, since blockade by EIPA indicated a significant reduction of NHE3 activity [44.2 ± 3.1% in Cre(−) and 42.5 ± 4.9% in Cre(+); Fig. 4], yet another NHE activity, which remained unaffected by EIPA, may have become acti-

vated upon GN induction. These changes were not influenced by megalin availability. BBM Western blot intensity mostly paralleled these changes (Fig. 5A; Table 3). Cortical mRNA levels were unchanged for NHE3, whereas NaPi-IIa and AQP1 showed a reduction in GN that did not depend on megalin (Table 4).

In aggregate, these results show that cortical NHE3 synthesis and BBM abundance are largely unaffected by proteinuria as well as megalin-dependent endocytosis, whereas NHE3 activity was reduced in GN. Contrastingly, the abundances of NaPi-IIa and AQP1 were mostly reduced under GN-associated proteinuria, even though megalin-deficient cells showed the established, relative signal enhancement for NaPi-IIa caused by its impaired retrieval (4), and the same applied to AQP1. The details of these changes are summarized in Table 5.

Abundances of distal tubular transporters and AQP2. To study the epithelial effects of GN on transporter proteins of the distal tubule and collecting duct, the expression and cellular distribution of NKCC2, α-ENaC, β-ENaC, γ-ENaC, α-NKA, and AQP2 were evaluated (Table 3). Western blot quantifications were performed in cortical or medullary extracts of the plasma membrane in analogy to the BBM fractions, since it was assumed that the abundance of these transporters at their site of action indicates their activation.

Negative results were obtained with NKCC2 and α-NKA. Cortical and medullary parts of TAL segments showed no

Table 2. *COX-2, renin, and plasma aldosterone concentration*

	Cre(−)	Cre(+)	Cre(−)/GN	Cre(+)/GN
COX-2/glomerulus, %	100.00±14.23	80.19±20.91	114.66±7.13	91.98±16.42
Renin/glomerulus, %	100.00±9.44	93.50±9.13	79.12±6.22	75.21±1.61
Aldosterone, pg/ml	535.17±175.16	250.73±48.36	248.42±109.80	629.47±145.60

Values are means ± SE. COX-2, cyclooxygenase 2. Immunohistochemical evaluation of tissue cyclooxygenase-2 (COX-2) and renin signals, and radioactive measurements of plasma aldosterone concentration are summarized in Table 3. No significant differences were observed.
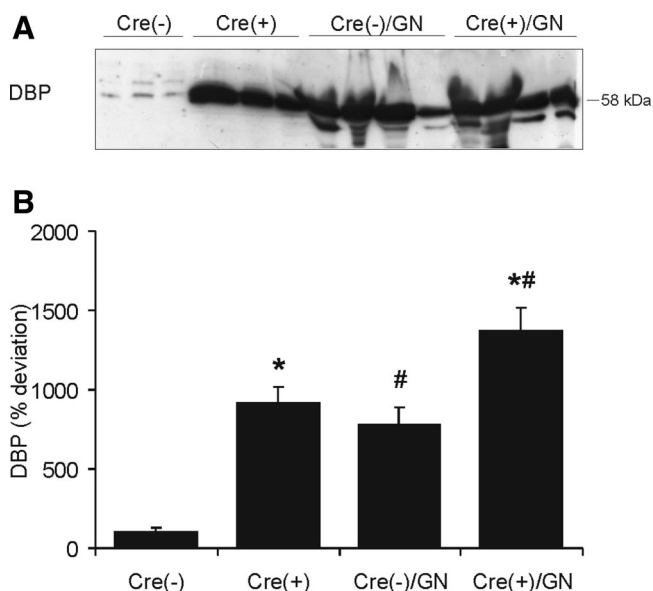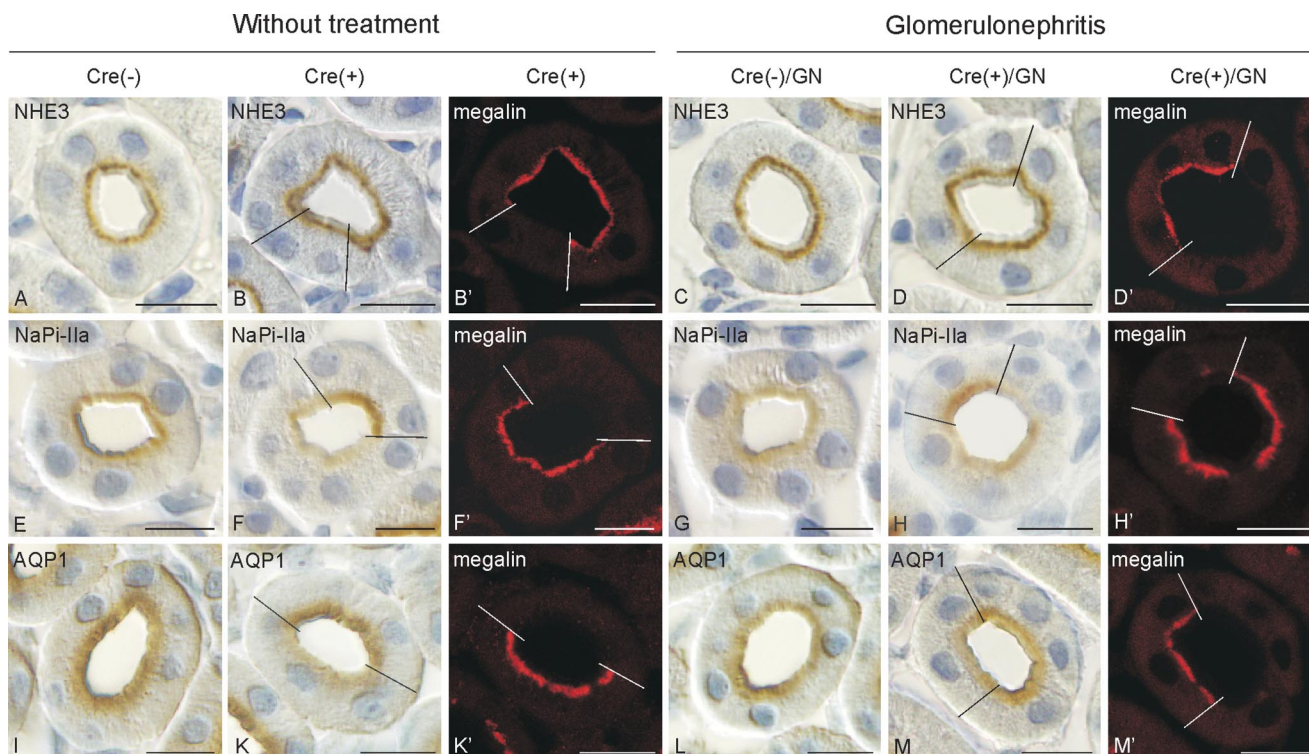
Without treatment

Glomerulonephritis

Fig. 3. Immunohistochemical staining of proximal tubular Na$^+$/H$^+$ exchanger 3 (NHE3), Na-P$_i$ cotransporter IIa (Na-Pi IIa), and aquaporin-1 (AQP1). Respective double labeling with anti-megalin is indicated by inverted comma (*A*, *B*, *E*, *F*, *I*, *K*). In control conditions, there are no changes for NHE3, whereas NaPi-IIa and AQP1 show increased BBM staining in megalin-deficient cells. (*C*, *D*, *G*, *H*, *L*, *M*). In GN, NHE3 staining is generally unaltered, whereas NaPi-IIa and AQP1 BBM staining is diminished. Six mice have been evaluated per group. Bars = 20 μm.

changes among all groups in NKCC2 plasma membrane abundance, and neither was total α-NKA altered in cortex or medulla (Table 3). In contrast, α-ENaC and γ-ENaC showed significant, selective enhancements not of their major, characteristic full-length bands, but of additional, lower molecular weight bands, which probably represented cleavage products of these ENaC subunits.
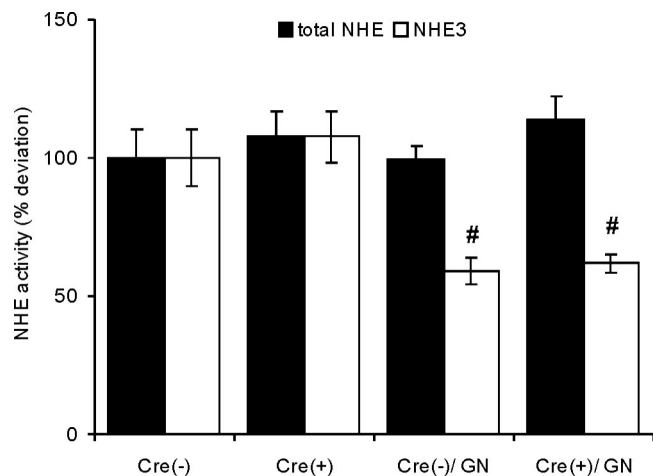

Fig. 4. NHE3 activity. NHE3 activity is expressed as variations in vesicular pH measured by the acridine orange quenching method. Filled bars, total NHE activity; open bars, specific NHE3 activity. In controls, total brush border membrane (BBM) NHE activity equaled specific NHE3 activity. In GN, NHE3 activity is strongly reduced in both groups. Values are means ± SE; n = 6. #P < 0.05 control vs. GN.

At steady state, the additional bands at ∼55 and 30 kDa were 3.74- and 1.26-fold enhanced for cortical α-ENaC in Cre(+) compared with Cre(−), suggesting that the absence of megalin and lack of proximal RME had led to a higher distal yield of filtered plasma components possibly acting on ENaC structure (Fig. 5*B*). Similarly, but less pronounced, an additional band for cortical γ-ENaC at 70 kDa was selectively stronger in Cre(+) (Fig. 5*B*). Additional α-ENaC bands in the medulla were enhanced as well (Fig. 5*C*). There were no changes in allover β-ENaC or medullary γ-ENaC expression (Table 3).

In GN, the 55- and 30-kDa band densities for cortical α-ENaC were 5.08- and 1.51-fold enhanced in Cre(−)/GN and 7.44- and 1.89-fold in Cre(+)/GN, respectively (Fig. 5*B*). For medullary α-ENaC, the 55- and 30-kDa band densities were 3.5- and 1.75-fold increased in Cre(−)/GN and 4.79- and 2.0-fold increased in Cre(+)/GN, respectively (Fig. 5*C*). These results thus further underline the impact of endocytosis on nephritis-grade distal tubular proteinuria and its possible modification of α-ENaC. Cortical γ-ENaC was also showing increases in the 70- and 55-kDa bands in GN, but the effects of endocytosis were not detectable [70 kDa: 2-fold increases in Cre(−)/GN and 2.2-fold in Cre(+)/GN; 55 kDa: 4.1- and 4.31-fold increases each in Cre(−)/GN and Cre(+)/GN]. Again, there were no changes in the medulla for γ-ENaC or in total β-ENaC expression (Table 3).

Expressed as total densities of the full-length and lower molecular weight bands, compared with Cre(−) the increases in Cre(+), Cre(−)/GN, and Cre(+)/GN were 4.16-, 4.76-, and 8.49-fold for cortical α-ENaC and 1.57-, 4.1-, and 5.76-fold for
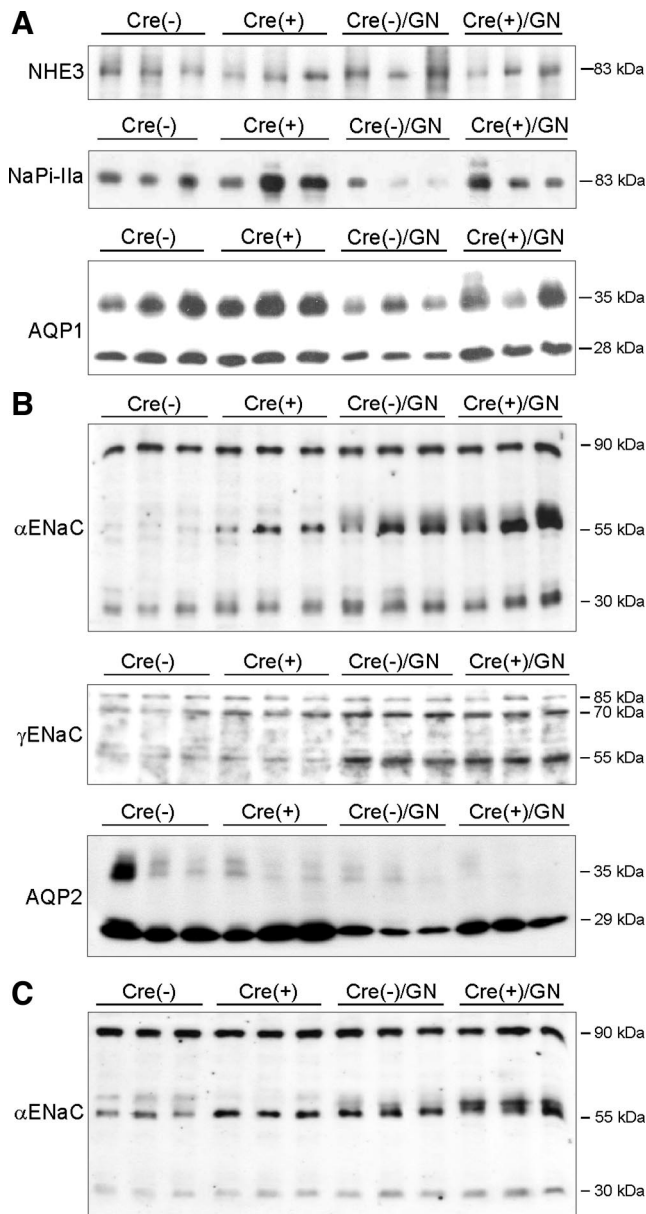
Fig. 5. Semiquantitative immunoblotting of altered sodium transporters and water channels along the nephron. *A*: proximal tubular BBM abundance of NHE3, NaPi-IIa, and AQP1. *B*: cortical plasma membrane abundance of α-epithelial Na channel (ENaC), γ-ENaC, and AQP2. The major (full-length) bands of α- and γ-ENaC as well as the smaller bands (putative cleavage products) are demonstrated. For AQP2, two major bands at 29 and 35 kDa are shown. *C*: medullary plasma membrane abundance of α-ENaC major and minor bands. All Western blots are representative results from 6 mice per group. Calculations of Western blot analysis are summarized in Table 3.

Table 3. *Protein abundances (Western blotting)*

	Calculations of Total Protein Abundance ± SE			
	Cre(−)	Cre(+)	Cre(−)/GN	Cre(+)/GN
BBM fraction				
NHE3	1.00±0.30	1.20±0.31	1.26±0.35	1.17±0.40
NaPi-IIa	1.00±0.53	2.19±0.29*	0.41±0.20	0.89±0.23†
AQP1	1.00±0.08	1.30±0.04*	0.65±0.10†	0.81±0.07†
Cortical PM fraction				
NKCC2	1.00±0.17	1.06±0.17	0.77±0.06	0.87±0.10
α-ENaC 90 kDa	1.00±0.08	1.16±0.16	1.17±0.05	1.22±0.13
α-ENaC 55 kDa	1.00±0.23	3.74±0.82*	5.08±0.11†	7.44±0.95*†
α-ENaC 30 kDa	1.00±0.08	1.26±0.02*	1.51±0.09†	1.83±0.07*†
β-ENaC	1.00±0.19	0.88±0.23	0.94±0.18	0.89±0.26
γ-ENaC 85 kDa	1.00±0.01	0.97±0.09	1.09±0.04	1.03±0.12
γ-ENaC 70 kDa	1.00±0.09	1.62±0.16*	2.00±0.12†	2.22±0.08†
γ-ENaC 55 kDa	1.00±0.13	1.41±0.50	3.01±0.17†	3.08±0.37†
α-Na-K-ATPase	1.00±0.25	1.06±0.18	1.09±0.17	0.96±0.20
AQP2	1.00±0.21	0.93±0.09	0.33±0.03†	0.35±0.08†
Medullary PM fraction				
NKCC2	1.00±0.40	0.86±0.17	1.76±0.37	1.34±0.24
α-ENaC 90 kDa	1.00±0.06	0.90±0.05	0.85±0.04	0.94±0.14
α-ENaC 55 kDa	1.00±0.10	1.41±0.10*	3.50±0.10†	4.79±0.15*†
α-ENaC 30 kDa	1.00±0.06	1.26±0.08*	1.75±0.05†	2.03±0.06*†
β-ENaC	1.00±0.10	1.05±0.09	0.94±0.25	1.50±0.35
γ-ENaC 85 kDa	1.00±0.09	1.03±0.12	0.99±0.16	1.02±0.12
γ-ENaC 70 kDa	1.00±0.23	1.06±0.04	1.10±0.11	1.18±0.03
γ-ENaC 55 kDa	1.00±0.17	1.10±0.12	1.17±0.13	1.18±0.13
α-Na-K-ATPase	1.00±0.11	1.37±0.14	1.25±0.22	0.95±0.17
AQP2	1.00±0.08	0.94±0.05	0.88±0.12	0.85±0.08

Values are means ± SE of densitometric intensity levels normalized to β-actin with Cre(−) set as 1 = 100%; $n = 6$. BBM, brush border membrane; NHE3, Na$^+$/H$^+$ exchanger 3; NaPi-IIa, Na$^+$-P$_i$ cotransporter IIa; ENaC, epithelial Na channel; AQP, aquaporin; PM, plasma membrane. Sources were BBM and PM. *$P < 0.05$ Cre(−) vs. Cre(+). †$P < 0.05$ control vs. GN.

The signals for AQP2 were strongly diminished in the cortex but not the medulla of Cre(−)/GN and Cre(+)/GN (Fig. 5*B*; Table 3).

These findings were roughly paralleled by changes registered in the immunohistochemical staining series (Fig. 6). The adluminal staining for cortical collecting duct α-ENaC and γ-ENaC was increased in Cre(+) compared with Cre(−). Cortical α-NKA and AQP2 signals were not markedly different between Cre(−) and Cre(+). In GN, Cre(+) showed stronger adluminal ENaC signals than Cre(−). α-NKA signals showed massive increases in GN; this differed from the Western blot analysis (Table 3), representing a mixture of all segments so that α-NKA changes in the collecting ducts were probably masked. AQP2 signals were diminished in the GN groups.

DISCUSSION

This study adds new insights to the discussion of whether primary, kidney-based salt and water retention, or other, sys-

medullary α-ENaC, respectively (each $P < 0.05$; Table 3), displaying significant increases also between Cre(−)/GN and Cre(+)/GN ($P < 0.05$). For cortical γ-ENaC, increases were 3.0-, 4.1-, and 4.31-fold in Cre(+), Cre(−)/GN, and Cre(+)/GN, respectively ($P < 0.05$; Table 3), but differences between Cre(−)/GN and Cre(+)/GN were not significant. Together, total density values indicate increased abundances of ENaC subunits in distal membranes as a function of different grades of proteinuria.

Table 4. *mRNA abundances of NHE3, NaPi-IIa, and AQP1*

	Calculations of Total mRNA Abundance ± SE			
	Cre(−)	Cre(+)	Cre(−)/GN	Cre(+)/GN
NHE3	1.00±0.11	0.99±0.23	0.95±0.23	1.16±0.10
NaPi-IIa	1.00±0.03	1.26±0.16	0.36±0.05*	0.48±0.09*
AQP1	1.00±0.11	1.05±0.18	0.35±0.14*	0.39±0.07*

Values are means ± SE; $n = 6$. Control levels Cre(−) are set as 1 = 100%. *$P < 0.05$ Cre(−) vs. Cre(+).

Table 5. *Summary of changes in proximal tubule transporter and channel parameters*

	Cre(+)	Cre(−)/GN	Cre(+)/GN
NHE3			
IHC	↔	↔	↔
Western blot			
BBM	↔	↔	↔
mRNA in cortex	↔	↔	↔
Activity in			
BBM	↔	↓	↓
NaPi-IIa, AQP1			
IHC	↑	↓	↔(↓ vs. Cre+)
Western blot			
BBM	↑	↓	↔(↓ vs. Cre+)
mRNA in cortex	↑	↓	↓

IHC, immunohistochemistry. Vertical arrows indicate significant changes. All changes refer to Cre(−) unless indicated separately.

temic causes prevail in the volume disorders accompanying heavy proteinuria. Our results have demonstrated that the blunted proximal RME and resulting mild proteinuria as well as the GN-induced glomerular proteinuria with or without proximal RME had little impact on proximal tubular membrane transporters with respect to volume retention. No changes were encountered in the loop of Henle. In contrast, both measures have caused major, in part additive, changes in surface expression and molecular weight shifts of ENaC subunits suggestive of channel activation and potential salt retention. Significant increases in blood pressure, decreased fractional sodium excretion, and increased plasma cholesterol levels were established in the GN groups. By stabilizing proteinuria within limits of 10–15 mg/24 h in these groups, we could avoid changes in GFR which occur with progressive glomerular and tubulointerstitial damage in the megalin-deficient group (22,

51) so that parameters related to sodium handling were comparable among groups.

With the bulk of sodium reabsorption occurring in the proximal tubule, this segment has been considered to efficiently contribute to volume retention as reported from a rat study with experimental nephrosis (7). Proximal tubular NHE3 is responsible for virtually all the local Na^+/H^+ exchange activity; it is the most effective proximal sodium transporter and furthermore plays a role in RME by its capacity to acidify endosomes for proper receptor-ligand dissociation (23). NHE3 activity can be estimated by its biosynthesis rate, its capacity to redistribute along the BBM microvilli (55), and its acidification capacity in BBM vesicles; the latter can also be used to measure its general activity (12). In our study, however, NHE3 failed to reveal major changes in these parameters except for the decrease in NHE3-specific BBM vesicular acidification in the GN groups. The decrease, however, appeared to be balanced by another, EIPA-resistant NHE isoform so that there was no general deficit in acidification of BBM vesicles. We therefore conclude that expression and activity of NHE3 were not megalin dependent and showed no changes with reduced RME. The drastic reduction of the proximal endosomal and recycling apparatus which otherwise influences NaPi-IIa retrieval (4) therefore does not seem to affect NHE3 expression.

The two other products of proximal BBM, NaPi-IIa and AQP1, showed similar results. Megalin deficiency per se caused a reduced retrieval of these products, leading to their increased abundance in BBM, which is consistent with earlier findings on NaPi-IIa expression (4). The GN groups showed decreased NaPi-IIa and AQP1 abundance and transcription rate, with immunoreactive signals equally reduced in megalin-positive and megalin-deficient proximal epithelia in the megalin-deficient group. These results partly agree with previous
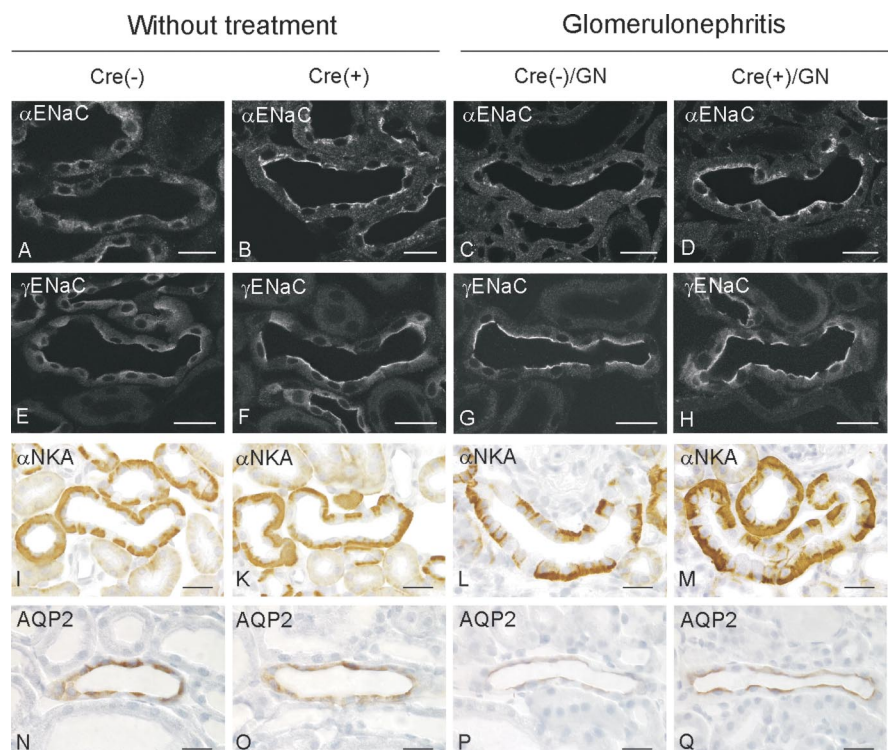

Fig. 6. Immunohistochemical staining of cortical α-ENaC, γ-ENaC, α-Na+-K+-ATPase (NKA), and AQP2. *A–H*: adluminal abundances for α-ENaC and γ-ENaC are increased in the Cre(+) controls and in both GN groups with strongest signals in Cre(+)/GN. *I–M*: basolateral α-NKA signals in GN are stronger than in controls. *N–Q*: AQP2 signals are diminished in the GN groups. Six mice have been evaluated per group. Bars = 20 μm.

work in models of nephrotic syndrome or anti-Thy1 GN (22, 33), although the reason for the decreases remains to be established. Functionally, the decrease in AQP1 and consequent reduction in proximal transcellular water passage may activate tubuloglomerular feedback, which prevents inadequate water and NaCl delivery to the distal nephron in AQP1-deficient mice (45). Feedback activation in nephrosis may be relevant to stabilize sodium and water delivery to the postmacula segments (29).

Taken together, neither the abundance nor the activity of NHE3, NaPi-IIa, and AQP1 in our model is consistent with proximal tubule-based volume retention in GN and is thus at variance with data raised in puromycin aminonucleoside nephrosis (7). Along the same line, earlier micropuncture studies in rats were not supporting a direct role for the proximal tubule in sodium retention. Studies on experimental anti-GBM nephritis demonstrated equal fractional reabsorption of the proximal tubule in controls and anti-GBM treated rats (46), and rats with unilateral nephrosis showed reduced sodium reabsorption in proximal convoluted tubule and thick ascending limb (29). The absence of changes in juxtaglomerular COX-2 (50) and RAAS parameters further underlines our conclusion and is partly consistent with previous work (8, 16, 22, 46).

The most striking results of this study are related to the collecting duct system. In megalin-deficient controls as well as in both GN groups alike, the plasma membrane abundances of α-ENaC and γ-ENaC revealed by Western blotting (sum of band densities) and immunohistochemistry were enhanced, suggesting that despite the major quantitative differences in urinary protein levels, decreased proximal RME and resulting tubular proteinuria as well as glomerular proteinuria were both producing similar changes in the adluminal collecting duct cell compartment. The reason for these trafficking events in the absence of RAAS changes is not clear. In nephrotic syndrome, an influence of altered tubular protein composition on the intracellular trafficking machinery in the absence of mineralocorticoid changes has been considered (3). The absence of changes in β-ENaC parallels other work on disproportionate changes of ENaC subunits in nephrosis, suggesting that β-ENaC is less involved in regulatory events (22, 32, 39).

The increased Western blot abundances of ENaC subunits in the membrane fractions were characterized by selective enhancements of the smaller 55- and 30-kDa bands for the α-subunit and 70 kDa for the γ-subunit in the cortex of megalin-deficient mice, whereas the full-length bands were not altered. These increases were more pronounced in the GN groups, chiefly for α-ENaC, which also showed enhanced medullary signals of the smaller bands. RME deficiency produced additive changes. Increases in the 70-kDa γ-ENaC bands in GN were restricted to the cortex and also revealed changes in a second 55-kDa band; both bands showed no further changes with reduced RME.

These results may be important in light of recent findings suggesting that ENaC electrophoretic shifts occur upon enzymatic cleavage of its subunits and that these changes are consistent with an activation of the channel (5, 25, 28, 44). This mechanism has been illustrated by the observation that amiloride-sensitive sodium currents are increased in response to extracellular serine protease (52), and exogenously added trypsin and resident proteases had similar effects (5, 25, 28). Inhibitory tracts of ENaC subunits, that can be liberated by

proteolysis, have further been identified (13). Proteases such as plasmin, which could be obtained from the urine of nephrotic rats, were shown to activate ENaC (43, 48). Plasmin may be locally activated from filtered plasminogen and appears to be particularly effective in full-channel activation by proteolytic processing of γ-ENaC (43). Passage of plasma proteases through the leaky glomerular filter in GN has been established, so that a similar mechanism of ENaC proteolysis and activation may be operative in our GN model. In the rat, we previously had obtained similar results in anti-Thy1 GN, with α-ENaC revealing an additional 65-kDa band typical of furin cleavage (22, 28). While the size of the present 70-kDa γ-ENaC cleavage product corresponds to published evidence (43), increases in α-ENaC bands were ranging at somewhat divergent molecular weight ranges compared with previous data. The larger 55-kDa band may be regarded as mildly divergent but analogous to otherwise shown 60- to 65-kDa ranges (22). The 30-kDa band suggests that the minor NH_2-terminal extracellular domain (and not the long 60-kDa major portion) of the cleaved protein was recognized, since our antibody was directed to an NH_2-terminal fusion protein and not to the COOH-terminally tagged recognition sites used by other groups; this agrees with previous data obtained with the NH_2-terminally directed antibody which recognized the 30-kDa band as well (19, 21, 44). The 30-kDa fragment also reflects furin (or other protease)-dependent cleavage under stimulated condition in a heterologous system (28). It may further be considered that the occurrence of the 55-kDa ranges for α- and γ-ENaC products could be related to immature or degraded glycosylation, possibly resulting from insufficient intracellular processing, or via the action of filtered glycosidases or locally activated deglycosylation (19). The concept of ENaC activation by proteolytic cleavage is thus indirectly supported by our results in GN-associated proteinuria. Loss of proximal RME per se was associated with marked increases in ENaC cleavage products, suggesting that the relevant proteases are ligands of megalin. Data further support, at least for α-ENaC, that depending on the extent of proteinuria and ensuing proximal saturation of RME, megalin may thus indirectly affect downstream sodium handling.

Our data thus support a role of the collecting duct system as the crucial site in the nephron for sodium retention in proteinuric nephropathy which agrees with earlier work (11, 29, 32, 33, 38, 46). Apart from the presumed role for ENaC, primary, aldosterone-independent involvement of NKA in distal sodium retention has further been discussed (7, 38). It must, however, be considered that an ENaC-mediated rise in intracellular sodium concentration may also per se adjust the activity of NKA (9). The observed immunohistochemical upregulation of collecting duct α-NKA would therefore agree with activated transport secondary to a rise in ENaC-mediated intracellular sodium concentration (38).

The marked decreases in AQP2 abundance in the GN groups also reflect earlier data from models of the nephrotic syndrome (20) and could represent a physiologically appropriate response to extracellular volume expansion. AQP2 may act independently of plasma vasopressin levels, which tend to be normal or elevated in these models (2, 19).

Since lipiduria is a frequent phenomenon in proteinuric disease and plasma cholesterol was enhanced in our model, altered membrane lipids may further be related to the observed

changes. Cellular fatty acids may cause cell dysfunction, and mice loaded with fatty acid and BSA exhibited systemic water retention (31) so that altered transepithelial reabsorption of sodium and water in the present model may be related to these changes. Since NaPi-IIa, NHE3, and aquaporins have been shown to be lipid raft associated, trafficking or membrane association of these proteins may be impaired in an altered cholesterol environment (10, 14, 30, 37, 41, 56). This may apply as well to distal epithelia, where NKA (53), NKCC2 (54), and ENaC (26) were shown to be partially lipid raft dependent, albeit with heterogenous functional consequences which are not entirely understood at present.

In sum, our study has identified renal changes in anti-GBM nephritis which may be relevant for volume retention, hypertension, and edema formation in human GN or nephritic syndrome. Our model suggests that in GN, altered filtrate composition as well as proximal tubular RME, controlled by megalin, are major determinants for renal-based salt retention and volume expansion. Whereas proximal tubular membrane transporters do not seem to be causally involved herein, structural changes in α- and γ-ENaC subunits, probably caused by proteolytic cleavage via filtered plasma proteases, as well as their enhanced membrane abundances may determine collecting duct-based sodium retention. Although tubular and glomerular proteinuria may produce analogous effects on sodium handling within distal epithelia, the effects of glomerular proteinuria clearly dominated those of blunted proximal endocytosis in contributing to ENaC cleavage and antinatriuresis.

REFERENCES

1. **Abbate M, Zoja C, Remuzzi G.** How does proteinuria cause progressive renal damage? *J Am Soc Nephrol* 17: 2974–2984, 2006.
2. **Apostol E, Ecelbarger CA, Terris J, Bradford AD, Andrews P, Knepper MA.** Reduced renal medullary water channel expression in puromycin aminonucleoside-induced nephrotic syndrome. *J Am Soc Nephrol* 8: 15–24, 1997.
3. **Audigé A, Yu ZR, Frey BM, Uehlinger DE, Frey FJ, Vogt B.** Epithelial sodium channel (ENaC) subunit mRNA and protein expression in rats with puromycin aminonucleoside-induced nephrotic syndrome. *Clin Sci* 104: 389–395, 2003.
4. **Bachmann S, Schlichting U, Geist B, Mutig K, Petsch T, Bacic D, Wagner CA, Kaissling B, Biber J, Murer H, Willnow TE.** Kidney-specific inactivation of the megalin gene impairs trafficking of renal inorganic sodium phosphate cotransporter (NaPi-IIa). *J Am Soc Nephrol* 15: 892–900, 2004.
5. **Bengrine A, Li J, Hamm LL, Awayda MS.** Indirect activation of the epithelial Na^+ channel by trypsin. *J Biol Chem* 282: 26884–26896, 2007.
6. **Bernard DB, Alexander EA, Couser WG, Levinsky NG.** Renal sodium retention during volume expansion in experimental nephrotic syndrome. *Kidney Int* 14: 478–485, 1978.
7. **Besse-Eschmann V, Klisic J, Nief V, Le Hir M, Kaissling B, Ambuhl PM.** Regulation of the proximal tubular sodium/proton exchanger NHE3 in rats with puromycin aminonucleoside (PAN)-induced nephrotic syndrome. *J Am Soc Nephrol* 13: 2199–2206, 2002.
8. **Bistrup C, Thiesson HC, Jensen BL, Skøtt O.** Reduced activity of 11beta-hydroxysteroid dehydrogenase type 2 is not responsible for sodium retention in nephrotic rats. *Acta Physiol Scand* 184: 161–169, 2005.
9. **Blot-Chabaud M, Jaisser F, Gingold M, Bonvalet JP, Farman N.** Na^+-K^+-ATPase-dependent sodium flux in cortical collecting tubule. *Am J Physiol Renal Fluid Electrolyte Physiol* 255: F605–F613, 1988.
10. **Bobulescu IA, Dubree M, Zhang J, McLeroy P, Moe OW.** Effect of renal lipid accumulation on proximal tubule Na^+/H^+ exchange and ammonium secretion. *Am J Physiol Renal Physiol* 294: F1315–F1322, 2008.
11. **Buerkert J, Martin DR, Trigg D, Simon EE.** Sodium handling by deep nephrons and the terminal collecting duct in glomerulonephritis. *Kidney Int* 39: 850–857, 1991.
12. **Cassano G, Stieger B, Murer H.** Na/H- and Cl/OH-exchange in rat jejunal and rat proximal tubular brush border membrane vesicles. Studies with acridine orange. *Pflügers Arch* 400: 309–317, 1984.
13. **Carattino MD, Hughey RP, Kleyman TR.** Proteolytic processing of the epithelial sodium channel γ subunit has a dominant role in channel activization. *J Biol Chem* 283: 25290–25295, 2008.
14. **Crane JM, Verkman AS.** Long-range nonanomalous diffusion of quantum dot-labeled aquaporin-1 water channels in the cell plasma membrane. *Biophys J* 94: 702–713, 2008.
15. **Christensen EI, Birn H.** Megalin and cubilin: multifunctional endocytic receptors. *Nat Rev Mol Cell Biol* 3: 256–266, 2002.
16. **Dechow C, Morath C, Peters J, Lehrke I, Waldherr R, Haxsen V, Ritz E, Wagner J.** Effects of all-*trans* retinoic acid on renin-angiotensin system in rats with experimental nephritis. *Am J Physiol Renal Physiol* 281: F909–F919, 2001.
17. **Doucet A, Favre G, Deschenes G.** Molecular mechanism of edema formation in nephrotic syndrome: therapeutic implications. *Pediatr Nephrol* 22: 1983–1990, 2007.
18. **Epstein AA.** Concerning the causation of edema in chronic parenchymatous nephritis; method for its alleviation. *Am J Med* 13: 556–561, 1952.
19. **Ergonul Z, Frindt G, Palmer LG.** Regulation of maturation and processing of ENaC subunits in the rat kidney. *Am J Physiol Renal Physiol* 291: F683–F693, 2006.
20. **Fernandez-Llama P, Andrews P, Ecelbarger CA, Nielsen S, Knepper M.** Concentrating defect in experimental nephrotic syndrome: altered expression of aquaporins and thick ascending limb Na^+ transporters. *Kidney Int* 54: 170–179, 1998.
21. **Frindt G, Ergonul Z, Palmer LG.** Surface expression of epithelial Na channel protein in rat kidney. *J Gen Physiol* 131: 617–627, 2008.
22. **Gadau J, Peters H, Kastner C, Kühn H, Nieminen-Kelhä M, Khadzhynov D, Krämer S, Castrop H, Bachmann S, Theilig F.** Mechanisms of tubular volume retention in immune-mediated glomerulonephritis. *Kidney Int.* In press.
23. **Gekle M, Drumm K, Mildenberger S, Freudinger R, Gassner B, Silbernagl S.** Inhibition of Na^+-H^+ exchange impairs receptor-mediated albumin endocytosis in renal proximal tubule-derived epithelial cells from opossum. *J Physiol* 520: 709–721, 1999.
24. **Gekle M.** Renal tubule albumin transport. *Annu Rev Physiol* 67: 573–594, 2005.
25. **Harris M, Firsov D, Vuagniaux G, Stutts MJ, Rossier BC.** A novel neutrophil elastase inhibitor prevents elastase activation and surface cleavage of the epithelial sodium channel expressed in *Xenopus laevis* oocytes. *J Biol Chem* 282: 58–64, 2007.
26. **Hill WG, Butterworth MB, Wang H, Edinger RS, Lebowitz J, Peters KW, Frizzell RA, Johnson JP.** The epithelial sodium channel (ENaC) traffics to apical membrane in lipid rafts in mouse cortical collecting duct cells. *J Biol Chem* 282: 37402–37411, 2007.
27. **Hricik DE, Chung-Park M, Sedor JR.** Glomerulonephritis. *N Engl J Med* 339: 888–899, 1998.
28. **Hughey RP, Mueller GM, Bruns JB, Kinlough CL, Poland PA, Harkleroad KL, Carattino MD, Kleyman TR.** Maturation of the epithelial Na^+ channel involves proteolytic processing of the α- and γ-subunits. *J Biol Chem* 278: 37073–37082, 2003.
29. **Ichikawa I, Rennke HG, Hoyer JR, Badr KF, Schor N, Troy JL, Lechene CP, Brenner BM.** Role for intrarenal mechanisms in the impaired salt excretion of experimental nephrotic syndrome. *J Clin Invest* 71: 91–103, 1983.
30. **Inoue M, Digman MA, Cheng M, Breusegem SY, Halaihel N, Sorribas V, Mantulin WW, Gratton E, Barry NP, Levi M.** Partitioning of NaPi cotransporter in cholesterol-, sphingomyelin-, and glycosphingolipid-en-

riched membrane domains modulates NaPi protein diffusion, clustering, and activity. *J Biol Chem* 279: 49160–49171, 2004.

31. **Kamijo Y, Hora K, Kono K, Takahashi K, Higuchi M, Ehara T, Kiyosawa K, Shigematsu H, Gonzalez FJ, Aoyama T.** PPARalpha protects proximal tubular cells from acute fatty acid toxicity. *J Am Soc Nephrol* 18: 3089–3100, 2007.

32. **Kim SW, Wang W, Nielsen J, Praetorius J, Kwon TH, Knepper MA, Frøkiær J, Nielsen S.** Increased expression and apical targeting of renal ENaC subunits in puromycin aminonucleoside-induced nephrotic syndrome in rats. *Am J Physiol Renal Physiol* 286: F922–F935, 2004.

33. **Kim SW, de Seigneux S, Sassen MC, Lee J, Kim J, Knepper MA, Frøkiær J, Nielsen S.** Increased apical targeting of renal ENaC subunits and decreased expression of 11βHSD2 in HgCl₂-induced nephrotic syndrome in rats. *Am J Physiol Renal Physiol* 290: F674–F687, 2006.

34. **Klisic J, Zhang J, Nief V, Reyes L, Moe OW, Ambühl PM.** Albumin regulates the Na^+/H^+ exchanger 3 in OKP cells. *J Am Soc Nephrol* 14: 3008–3016, 2003.

35. **Kuusniemi AM, Lapatto R, Holmberg C, Karikoski R, Rapola J, Jalanko H.** Kidneys with heavy proteinuria show fibrosis, inflammation, and oxidative stress, but no tubular phenotypic change. *Kidney Int* 68: 121–132, 2005.

36. **Leheste JR, Melsen F, Wellner M, Jansen P, Schlichting U, Renner-Müller I, Andreassen TT, Wolf E, Bachmann S, Nykjaer A, Willnow TE.** Hypocalcemia and osteopathy in mice with kidney-specific megalin gene defect. *FASEB J* 17: 247–249, 2003.

37. **Levi M, Baird BM, Wilson PV.** Cholesterol modulates rat renal brush border membrane phosphate transport. *J Clin Invest* 85: 231–237, 1990.

38. **Lourdel S, Loffing J, Favre G, Paulais M, Nissant A, Fakitsas P, Creminon C, Féraille E, Verrey F, Teulon J, Doucet A, Deschenes G.** Hyperaldosteronemia and activation of the epithelial sodium channel are not required for sodium retention in puromycin-induced nephrosis. *J Am Soc Nephrol* 16: 3642–3650, 2005.

39. **Masilamani S, Wang X, Kim GH, Brooks H, Nielsen J, Nielsen S, Nakamura K, Stokes JB, Knepper MA.** Time course of renal Na-K-ATPase, NHE3, NKCC2, NCC, and ENaC abundance changes with dietary NaCl restriction. *Am J Physiol Renal Physiol* 283: F648–F657, 2002.

40. **Motoyoshi Y, Matsuaka T, Saito A, Pastan I, Willnow TE, Mizutani S, Ichikawa I.** Megalin contributes to the early injury of proximal tubule cells during nonselective proteinuria. *Kidney Int* 74: 1262–1269, 2008.

41. **Murtazina R, Kovbasnjuk O, Donowitz M, Li X.** Na^+/H^+ exchanger NHE3 activity and trafficking are lipid Raft-dependent. *J Biol Chem* 281: 17845–17855, 2006.

42. **Orth SR, Ritz E.** [Nephrotic syndrome.] *Internist (Berl)* 39: 1246–1252, 1998.

43. **Passero CJ, Mueller GM, Rondon-Berrios H, Tofovic SP, Hughey RP, Kleyman TR.** Plasmin activates epithelial Na^+ channels by cleaving the γ subunit. *J Biol Chem* 283: 36586–36591, 2008.

44. **Rossier BC, Stutts MJ.** Activation of the epithelial sodium channel (ENaC) by serine proteases. *Annu Rev Physiol.* In press.

45. **Schnermann J, Chou CL, Ma T, Traynor T, Knepper MA, Verkman AS.** Defective proximal tubular fluid reabsorption in transgenic aquaporin-1 null mice. *Proc Natl Acad Sci USA* 95: 9660–9664, 1998.

46. **Simon EE, Merli C, Fry B, Buerkert J.** Contribution of superficial nephron segments to sodium excretion in experimental glomerulonephritis. *Kidney Int* 36: 601–608, 1989.

47. **Stauss HM, Gödecke A, Mrowka R, Schrader J, Persson PB.** Enhanced blood pressure variability in eNOS knockout mice. *Hypertension* 33: 1359–1363, 1999.

48. **Svenningsen P, Bistrup C, Friis UG, Bertog M, Haerteis S, Krueger B, Stubbe J, Jensen ON, Thiesson HC, Uhrenholt TR, Jespersen B, Jensen BL, Korbmacher C, Skøtt O.** Plasmin in nephrotic urine activates the epithelial sodium channel. *J Am Soc Nephrol* 20: 233–234, 2009.

49. **Theilig F, Câmpean V, Paliege A, Breyer M, Briggs JP, Schnermann J, Bachmann S.** Epithelial COX-2 expression is not regulated by NO: colocalization studies in rat and mouse renal cortex. *Hypertension* 39: 848–853, 2002.

50. **Theilig F, Debiec H, Nafz B, Ronco P, Nüsing R, Seyberth W, Pavenstädt H, Bouby N, Bachmann S.** Renal cortical regulation of COX-1 and functionally related products in early renovascular hypertension (rat). *Am J Physiol Renal Physiol* 291: F987–F994, 2006.

51. **Theilig F, Kriz W, Jerichow T, Schrade P, Hähnel B, Willnow T, Le Hir M, Bachmann S.** Abrogation of protein uptake through megalin-deficient proximal tubules does not safeguard against tubulointerstitial injury. *J Am Soc Nephrol* 18: 1824–1834, 2007.

52. **Vallet V, Chraibi A, Gaeggeler HP, Horisberger JD, Rossier BC.** An epithelial serine protease activates the amiloride-sensitive sodium channel. *Nature* 389: 607–610, 1997.

53. **Welker P, Geist B, Frühauf JH, Salanova M, Groneberg DA, Krause E, Bachmann S.** Role of lipid rafts in membrane delivery of renal epithelial Na^+-K^+-ATPase, thick ascending limb. *Am J Physiol Regul Integr Comp Physiol* 292: R1328–R1337, 2007.

54. **Welker P, Böhlick A, Mutig K, Salanova M, Kahl T, Schlüter H, Blottner D, Ponce-Coria J, Gamba G, Bachmann S.** Renal Na-K-Cl cotransporter activity and vasopressin-induced trafficking are lipid raft dependent. *Am J Physiol Renal Physiol* 295: F789–F802, 2008.

55. **Yang LE, Leong PK, McDonough AA.** Reducing blood pressure in SHR with enalapril provokes redistribution of NHE3, NaPi2, and NCC and decreases NaPi2 and ACE abundance. *Am J Physiol Renal Physiol* 293: F1197–F1208, 2007.

56. **Zager RA, Johnson AC, Hanson SY, Shah VO.** Acute tubular injury causes dysregulation of cellular cholesterol transport proteins. *Am J Pathol* 163: 313–320, 2003.